An Integrated Approach for Characterization and Modeling of Soft Clays under Seismic Loading: A Case Study

T. Durgunoglu[1], O. Yilmaz[2] , M. Kalafat[3] , T. Karadayilar[4] , M. Eser[5]
[1]Department of Civil Engineering, Bogazici University, Istanbul, Turkey
[2]Anatolian Geophysical, Istanbul, Turkey
[3]Department of Civil Engineering, Bogazici University, Istanbul, Turkey
[4]Zetas Zemin Teknolojisi AS, Istanbul, Turkey
[5]Anatolian Geophysical, Istanbul, Turkey

Abstract— **Saturated soft soils develop pore water pressure and strains when subjected to cyclic loadings that originate from earthquakes, traffic waves, and other sources of vibrations. Increase in pore pressure decreases the shear strength resulting stability problems including bearing capacity and flow failure, and causes modulus degradation and residual vertical displacements. Evaluation of such soils requires the evaluation of dynamic behavior. In this study, the geotechnical modeling of normally consolidated soft clays is investigated for a site in Riva, Istanbul where a major housing project is planned to be developed following an integrated approach. For this purpose borehole, geophysical and laboratory data obtained and evaluated together to obtain representative characterization of soft clays in this region. The low values of S-wave velocities indicate that the encountered soft clays are susceptible to soil amplification and liquefaction. Therefore, additional cyclic triaxial tests are performed on undisturbed samples obtained by piston samplers considering the high sensitivity of these clays for further assessment of liquefaction potential and cyclic mobility. It is shown that Chinese criteria is not applicable and such sensitive soft clays conforming to Youd's criteria exhibit considerable strength loss and vertical displacements under cyclic loading.**

Keywords— **Amplification and liquefaction, seismic loading, soft clays.**

INTRODUCTION

An integrated approach for the characterization and geotechnical modeling of soft clays for a major housing project are presented in this paper. The subject site is located in Riva, north of Istanbul and covers an area of approximately 1,500,000 m2. It lies within an alluvial flood plain formed by a tributary of Riva river, 3 km south of the Black Sea shore near Istanbul. The soil profile consists of Holocene aged and recent alluvial sediments of soft silty clays with interlayers of sand.

The integrated apprach consisted of combination of geophysical investigation methods for the characterization of soil in three dimensions throughout the site, associated with comprehensive investigation methods including electrical Cone Penetration Tests (CPT), seismic CPT, rotary boreholes, undistured sampling by means of piston sampler, field vane testing and laboratory testing, including cyclic triaxial behavior of soft silty clays.

THE SEISMIC SURVEY

A shallow seismic survey was conducted over the site of investigation to derive a 'seismic model' of the soil column and the underlying bedrock. The seismic model is defined by three sets of parameters --- geometry of the layers within the soil column and the soil-bedrock interface, and the P- and S-wave velocities of the layers themselves.

Fig. 1 shows the base map for the seismic survey. Multichannel seismic data were recorded along three reflection traverses (S1, S2, and S3) and three refraction traverses (S3A, S4A, and S4B) using a 48-channel recording system with 10-Hz geophones and an explosive source that uses a pipe-gun with three 50-gram shells placed in a 30-cm hole. Both the receiver and shot station intervals are 5 m. Common-spread recording geometry was used to record the data. Specifically, the receiver stations were kept the same for all shots, while the shots themselves were moved starting from one end of the line to the other.

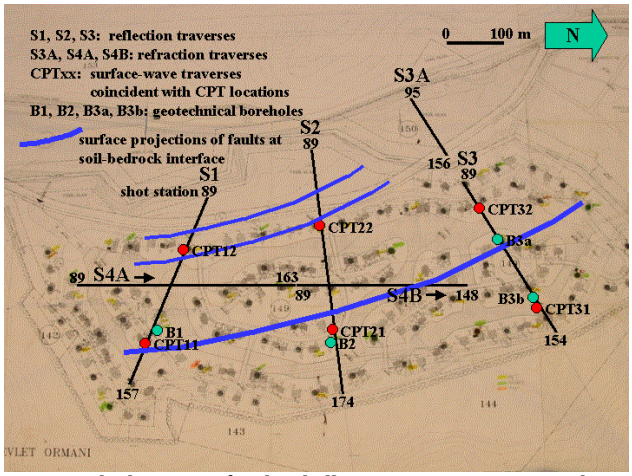

Fig. 1. The base map for the shallow seismic survey. Numbers represent the first and last shot points along the seismic lines.

Additionally, at six locations as indicated in Fig. 1 (CPT11, CPT12, CPT21, CPT22, CPT31, and CPT32), small-receiver spreads with 2-m receiver interval and 4.5-Hz geophones were used to acquire shot records for surface-wave analysis.

Fig. 2 shows an example of a field record that exhibits a set of good reflections, excellent first breaks associated with the refracted arrivals, and a dispersive wave package associated with the Rayleigh-type surface waves.

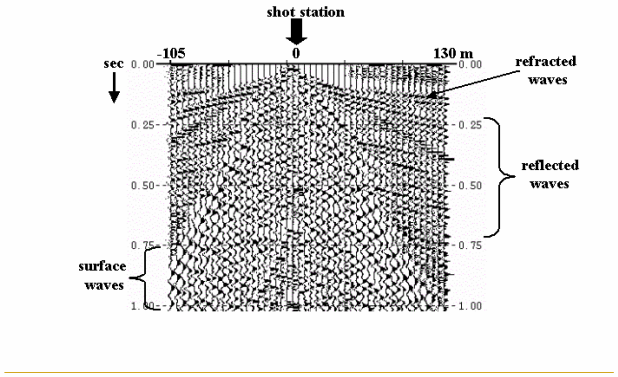

Fig. 2. A field record that exhibits reflected, refracted, and surface waves.

SEISMIC DATA ANALYSIS

A unified workflow [1] was applied to analyze the recorded seismic data. Specifically, by means of making use of reflected, refracted, and surface waves to estimate the seismic model of the soil column and the underlying bedrock within the survey site.

(1) A simple conventional processing sequence was appiled to shot gathers along each of the reflection traverses S1, S2, and S3 (Fig. 1) to obtain a CMP stack associated with the reflected waves.

(2) Inversion of travel times associated with the refracted waves in the recorded data was perfromed to estimate a near-surface P-wave velocity-depth model along each of the reflection (S1, S2, and S3) and refraction traverses (S3A, S4A, and S4B) and it was used to guide the interpretation of the CMP stack section to delineate the geometry of the layers within the soil column and the geometry of the soil-bedrock interface.

(3) Inversion of Rayleigh waves in the recorded data at each of the CPT locations (Fig. 1) was performed to derive an S-wave velocity-depth profile.

Analysis sequence for reflected waves includes low-cut filter to reject surface waves, amplitude scaling, normal-moveout correction to zero source-receiver separation and common-midpoint stacking [2]. Fig. 3a, 4a, and 5a show the reflection seismic sections for Lines S1, S2, and S3, respectively.

Analysis of refracted waves includes picking of first arrival times, building an initial, simple one-dimensional P-wave velocity-depth model, computing the refraction travel times associated with the initial model, perturbing the velocity-depth model based on a nonlinear travel time tomography until the difference between the modeled and the actual picked travel times is minimum so as to obtain a final velocity-depth model [3]. Fig. 3b, 4b, 5b, 6, and 7 show the P-wave velocity-depth models for Lines S1, S2, S3, S3A and S3 combined, and S4A and S4B combined, respectively.

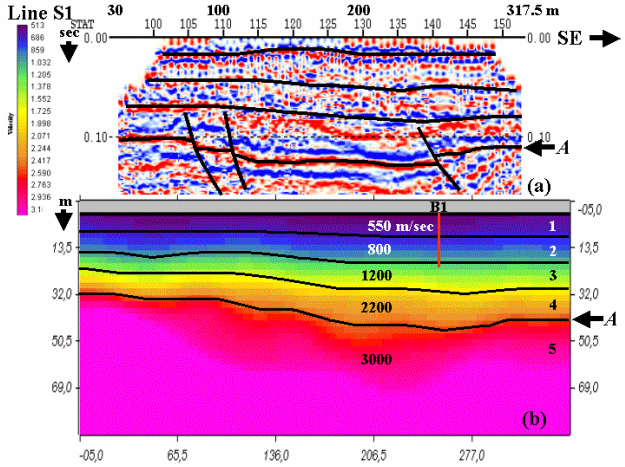

Fig. 3. Combined interpretation of the CMP stack (a) and P-wave velocity-depth model (b) for Line S1. A denotes the soil-bedrock interface.

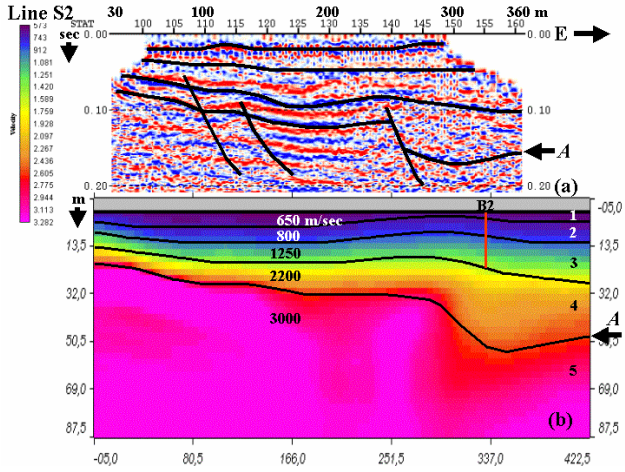

Fig. 4. Combined interpretation of the CMP stack (a) and P-wave velocity-depth model (b) for Line S2. A denotes the soil-bedrock interface.

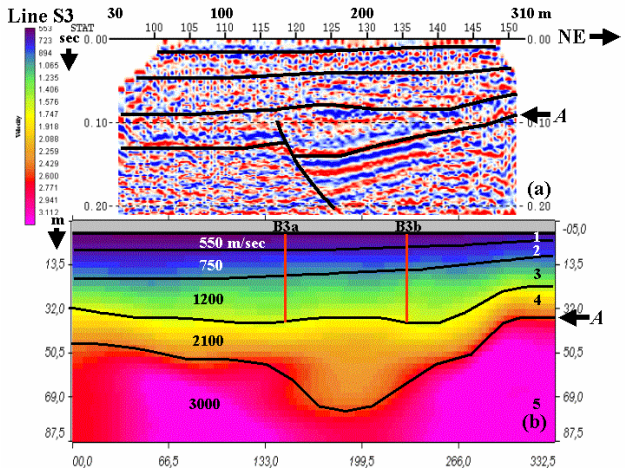

Fig. 5. Combined interpretation of the CMP stack (a) and P-wave velocity-depth model (b) for Line S3. A denotes the soil-bedrock interface.

Analysis of surface waves includes isolating the dispersive wave package on the shot record by muting, plane-wave decomposition by transforming the data from offset domain to ray-parameter domain, computing the amplitude spectrum of each of the plane-wave components, interpreting the resulting spectra for the phase-velocity curve for the fundamental mode of Rayleigh waves, and finally, inverting it to estimate an S-wave velocity-depth profile [4]. Fig. 8, 9, and 10 show the S-wave velocity-depth profiles estimated at six CPT locations on Lines S1, S2, and S3.

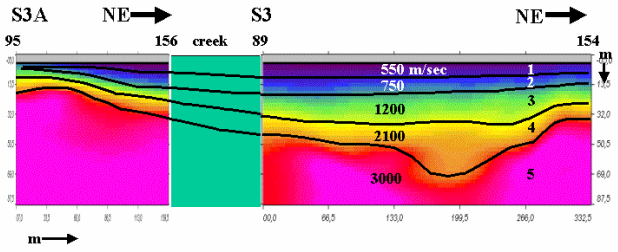

Fig. 6. Combined interpretation of the P-wave velocity-depth models for Lines S3A and S3.

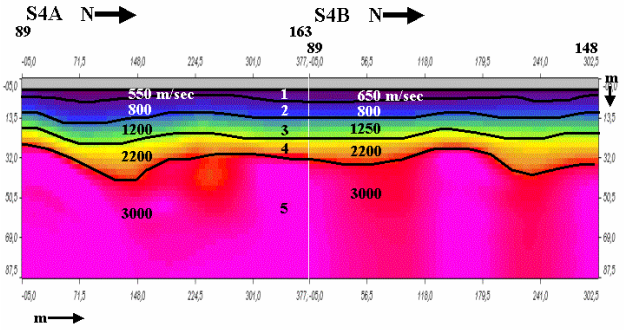

Fig. 7. Combined interpretation of the P-wave velocity-depth models for Lines S4A and S4B.

SEISMIC INTERPRETATION

We now combine the results of the analysis of reflected, refracted, and surface waves to derive the seismic model for the soil column and the bedrock.

(1) The interpretation of the reflection seismic sections (Fig. 3a, 4a, and 5a) combined with the P-wave velocity-depth models (Fig. 3b, 4b, and 5b) suggests a soil column with four layers with significant velocity contrast. For the alluvial basin that underlies the survey site we have similarly interpreted the P-wave velocity-depth models associated with the refraction traverses (Fig. 6 and 7). By using the color bar for the velocities, we have assigned average P-wave velocities for each of the layers as denoted in Fig. 3b, 4b, 5b, 6, and 7. Average P-wave velocities for layers 1, 2, 3, and 4 are 600, 800, 1,200, and 2,200 m/s, while the metamorphosed volcanic bedrock velocity is 3,000 m/s.

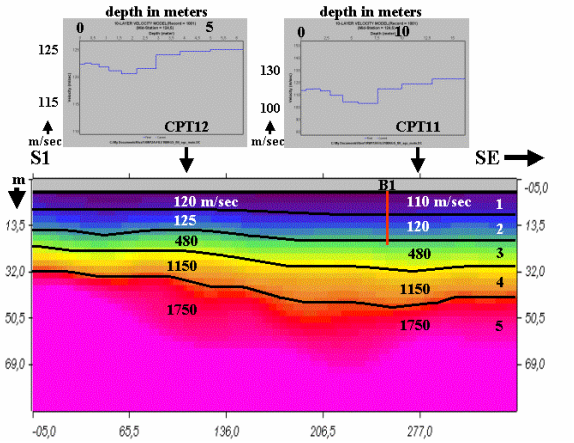

Fig. 8. Combined interpretation of the S-wave velocity-depth profiles (top) and the P-wave velocity-depth model (Fig. 4b) to derive an S-wave velocity-depth model for Line S1.

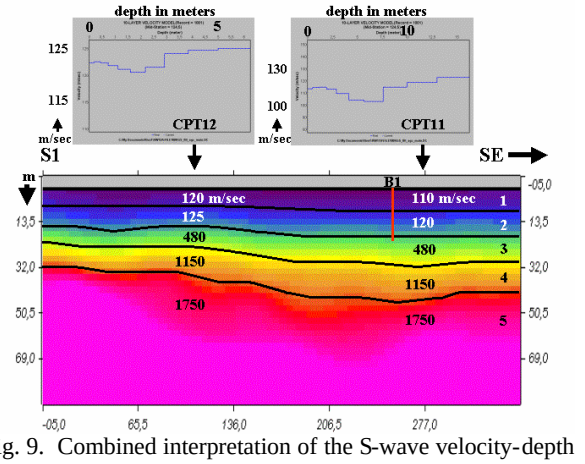

Fig. 9. Combined interpretation of the S-wave velocity-depth profiles (top) and the P-wave velocity-depth model (Fig. 5b) to derive an S-wave velocity-depth model for Line S2.

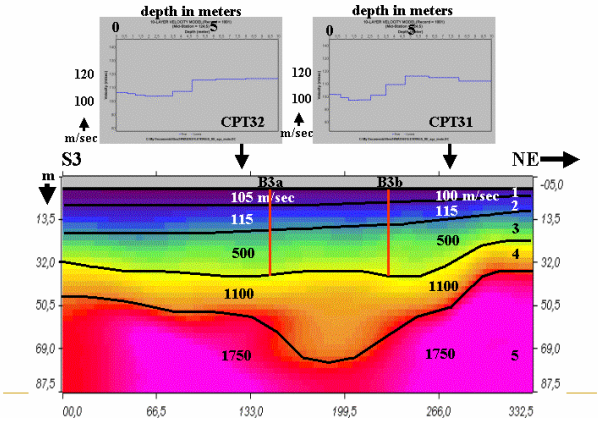

Fig. 10. Combined interpretation of the S-wave velocity-depth profiles (top) and the P-wave velocity-depth model (Fig. 5b) to derive an S-wave velocity-depth model for Line S3.

(2) Geotechnically, the velocity for layer 4 (2,200 m/s) may be considered as sufficiently high. Additionally, the velocity contrast between layer 3 (1,200 m/s) and 4 (2,200 m/s) is significant. As such, the boundary between layers 3 and 4 may be considered as the geotechnical soil-bedrock interface. In contrast, the geologic soil-bedrock interface corresponds to the interface between layers 4 and 5. The geotechnical soil-bedrock interface has an irregular geometry with depths varying between 15-40 m.

(3) The total depth for geotechnical borehole B1 coincides with the boundary between layers 2 and 3, whereas the total depths for B2, B3a, and B3b coincide with the geotechnical soil-bedrock interface (Fig. 3b, 4b, and 5b).

(4) The geologic soil-bedrock interface has been subjected to normal faulting in the past. The surface projection of the fault system is shown in Fig. 1. It appears not to have disturbed the alluvial soil column above, and thus, may be treated as an inactive fault system (Fig. 3, 4, and 5).

(5) The results of Rayleigh-wave inversion at CPT locations indicate that the S-wave velocity over the site is within the range of 100-125 m/s for the first 15-m of the soil column that includes layers 1 and 2 (Fig. 8, 9, and 10). If we consider an average P-wave velocity of 650 m/s for the first two layers (Fig. 3b, 4b, and 5b), then, the ratio of the P-wave velocity to the S-wave velocity for the first 15-m of the soil column is about 5.5.

GEOTECHNICAL INVESTIGATION CAMPAIGN

The seismic survey revealed that a comprehensive subsoil investigation campaign needed to be conducted within the subject site is composed of electrical Cone Penetration Tests, rotary boreholes, undisturbed piston sampling and laboratory testing. The thickness of soft alluvial layers overlying the basaltic bedrock reaches to 35.0 m depth in the central portion of the site. A typical seismic CPT record at the site, with variation of tip resistance q_c, sleeve friction f_s, friction ratio R_f, and shear wave velocity Vs with depth is given in Figure 11.

The measured shear wave velocities for the first 15m depth are in the range of 100-125 m/sec except at few locations which agrees very well with the values obtained by means of Rageigh wave inversion technique. Groundwater table is at a depth of 0.5 m below the ground surface. The site is within the second degree (second highest risk group) earthquake zone according to 1998 earthquake specification of Turkey. The cyclic triaxial testing programme is planned towards a better understanding of the soil behavior under possible seismic loading. Therefore in order to investigate the effect of dynamic excitement on the excess pore water development and dynamic shear modulus for clays, a series of cyclic undrained triaxial tests were performed on Riva clay.

Undisturbed soil samples have been obtained in the course of borings at the site. All samples have been retrieved from the field by means of fixed piston samplers [5]. Sampling tubes having an internal diameter of D=54mm were carefully cleaned and checked for defects before use. After retrieval of the sample, a preliminary identification was done, and then the ends of the tube were covered with paraffin to preserve the original moisture content. Tubes are carefully handled not to induce disturbing vibrations during transportation to the laboratory.

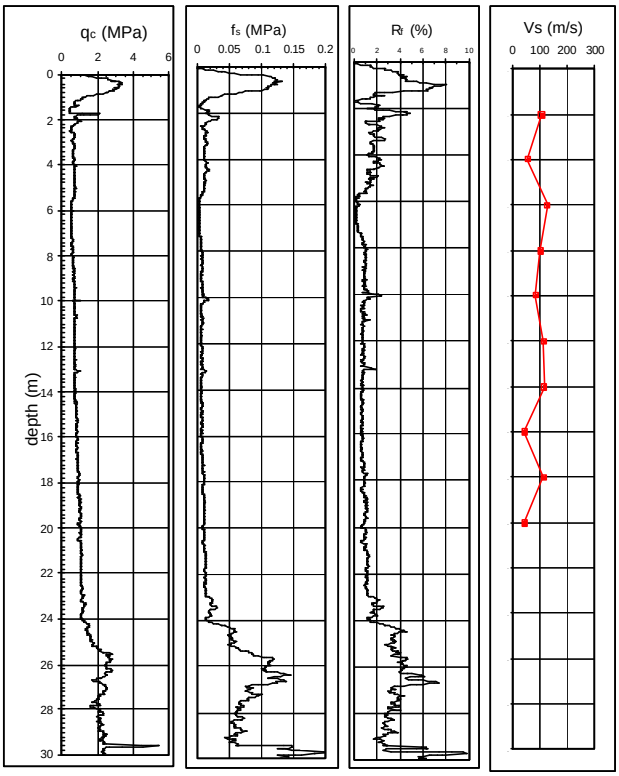

Fig. 11. A typical S-CPT record.

In the laboratory, samples were extracted from the tubes by a vertical oil piston sample extruder. Trimming was avoided to prevent disturbance. Vacuum saturation and back pressure saturation procedures were utilized successively to ensure saturation. For all samples a B value of at least 0.98 was achieved.

CYCLIC TRIAXIAL TESTING

Cyclic triaxial tests are often used to determine soil behavior under dynamic loading in the laboratory. Stress controlled cyclic tests were performed on CKC Automatic Cyclic Triaxial Testing setup [6]. During the tests, time, deviator stress, axial strain, cell pressure, effective pressure, and volumetric strain were automatically measured and recorded by equipment using the three pressure transducers, one load cell and one LVDT [12]. A sample test output can be seen in Figure 12.

After saturation and consolidation phase, cyclic deviator stresses ($\sigma_{d\text{-}cyc}$) were applied at 1Hz frequency.

In this study, cyclic stress ratio for specimens tested in triaxial test setup (CSR_{tx}) is defined as the ratio of cyclic shear stress on the sample ($\sigma_{d\text{-}cyc}$ /2) to effective mean consolidation stress (σ'_m). Since all of the samples are isotropically consolidated (no initial shear stress on the sample), CSR_{tx} becomes:

$$CSR_{tx} = \frac{s_{d-cyc}}{2 \cdot s'_{3c}}$$

where σ'3c is effective lateral consolidation pressure. Due to differences in the stress path and the nature of laboratory testing procedures, cyclic stress ratio are corrected as $CSR_{field} = 0.9 \cdot c_r \cdot CSR_{triaxial}$, where the average value of the correction factor c_r is 0.7 for various normally consolidated fine grained soils [7].

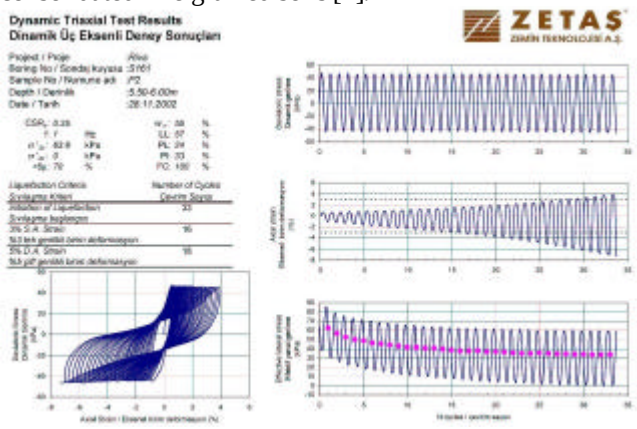

Fig. 12. Sample output of a cyclic triaxial test

A total of eight cyclic undrained triaxial tests were performed on silty clays obtained from seven different sample tubes. Plasticity, water content, sieve analysis, and hydrometer tests were performed for each sample. Index properties of the samples and in situ test results are summarized in Table 1.

Table 1. Properties of the test samples

Test No*	USCS	Depth (m)	Z_{gw} (m)	LL (%)	PI (%)	ω_n (%)	FC (%)	<5μ (%)	N_{SPT}	q_n (MPa)	c_u (kPA) Peak	c_u (kPA) Res.	S
1	CH	4.00-4.50	0.60	47	23	38	92	40	4	0.23	-	-	-
2	CH	7.00-7.50	0.60	43	21	37	98	40	3	0.48	-	-	-
3	CH	9.50-10.00	1.00	52	32	45	85	24	2	0.53	45	9	5
4	CH	5.50-6.00	1.20	57	33	55	100	70	2	0.85	20	2	10
6, 7	CH-MH	5.00-5.50	1.20	72	38	96	100	55	4	0.87	16	2	8
8	CH	5.00-5.50	1.75	57	31	50	100	65	6	0.43	27	4	7
9	CH-CL	6.50-7.00	1.75	49	26	47	88	65	4	0.83	58	6	12
Max				43	21	37	85	24	6	0.87	58	9	12
Ave				56	30	58	95	52	4	0.61	30	4	8
Min				72	38	96	100	70	2	0.23	16	2	5

USCS : Unified soil classification system
LL, PL : Liquid limit, Plastic limit
ω_n : Natural water content
FC : Fines content
<5μ : Particles finer than 5μ
N_{SPT} : SPT blow count
q_n : Net cone tip resistance
c_u : Undrained shear strength from in situ vane test
S : Sensitivity determined from in situ vane shear test
* Test 5 was performed on silty sand.

The triggering of liquefaction is represented in terms of number of uniform, constant amplitude cycles required to reach one of the following conditions during the test: 3% single amplitude axial strain, 5% double amplitude axial strain or zero effective lateral stress.

The variation of cyclic strength (N_f, number of cycles to failure) with respect to CSRtx is shown in Figure 13. N_f is selected as the minimum of number of cycles required to produce cyclic liquefaction. It could be seen from this figure that the cyclic liquefaction condition was reached in all tests except one sample with high plasticity values (i.e. LL=72, PI=38).

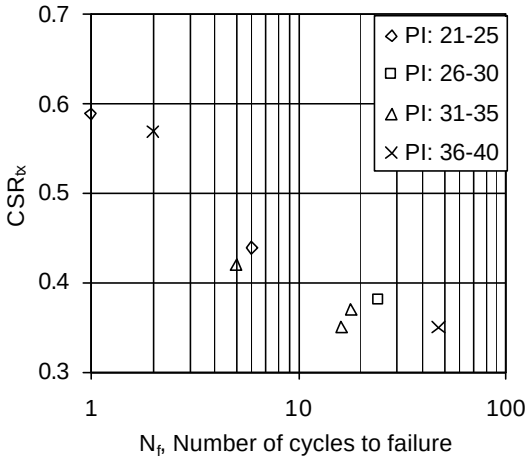

Fig. 13. Number of cycles required to reach failure condition

Development of residual pore water pressure is plotted in Figure 14. The amount of developed pore water pressure increases with increasing number of cycles and amplitude of loading. The relation between Δu_N and log(N) is approximately linear. However, it is known that pore pressure measurements are difficult in cyclic testing of materials with low permeability [8]. It is also generally observed during the testing that the cyclic strain increases significantly before the excess pore water pressure reaches the initial confining stress level.

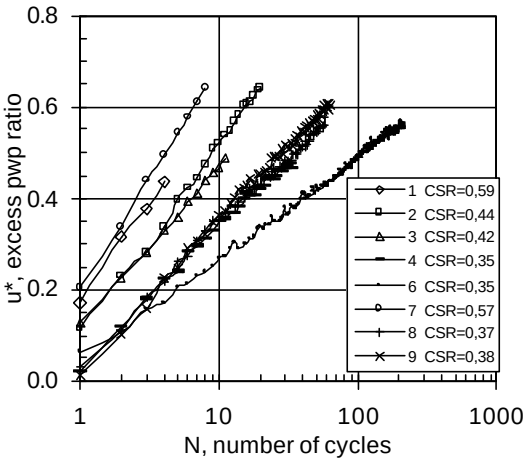

Fig. 14. Generation of residual pore water pressure

IMPLICATIONS AND CONCLUDING REMARKS

Seed and Idriss [9] developed a criteria called as Chinese criteria for clayey soils subjected to liquefaction based on the data obtained from the earthquakes in China. According to these criteria a clayey soil can liquefy under seismic loading if all of the following conditions are satisfied :

- Particles finer than 5μm < 15%
- LL < 35%
- ωn / LL > 0.9

According to the results of the performed cyclic triaxial tests, Riva clay under study did not conform with the Chinese criteria as could be seen from the Figure 15. Youd [10] stated that the Chinese criteria are reliable for predicting liquefaction of fine grained sediments but are generally conservative. However, the criteria do not work for sensitive soils. Thus, the plastic and clayey soils are also susceptible to liquefaction or cyclic mobility develops associated with a strength degradation if they are sensitive and may develop excess deformations and loose strength during the earthquakes. Youd [10] proposed the criteria as shown in the second column of the Table 2 for detecting the sensitivity for seismically induced strength loss. As could be seen from the third column on the same Table, Riva clay conforms with these criteria.

Table 2. Youd (1998)'s Criteria for sensitive clays subjected to excessive deformation and strength loss during/after seismic excitation

Criteria	Youd (1998)	Riva clay
Soil Types	CL or ML	CL, CH
Sensitivity	>4	5-12
Liquidity index	>0.6	0.6-1.6
Moisture content	>0.9xLL	(0.8-1.3)xLL
Penetration resistance	$(N_1)_{60}<5$ or $q_{clo}<1$Mpa	$(N_1)_{60}<5$, $q_{clo}<1$Mpa

Sancio et al. [11] have found based on a large number of cyclic triaxial tests performed on "undisturbed" specimens of Adapazari that the soils with PI>12, which generally have LL>35 can generate significant strains in a small number of cycles when a high CSR is applied on the contrary of the Chinese criteria. It is noted that the laboratory testing is essential for the soft silty clays with high plasticity to assess the cyclic liquefaction susceptibility.

Consquently, it should also be noted that for soft clays with shear wave velocities as low as Vs<200 m/s, it is deemed necessary to perform an integrated approach associated with geophysical methods, borings and CPT for characterization and modeling of soft clays and cyclic triaxial testing on undisturbed samples for a better understanding of behaviour under seismic loading.

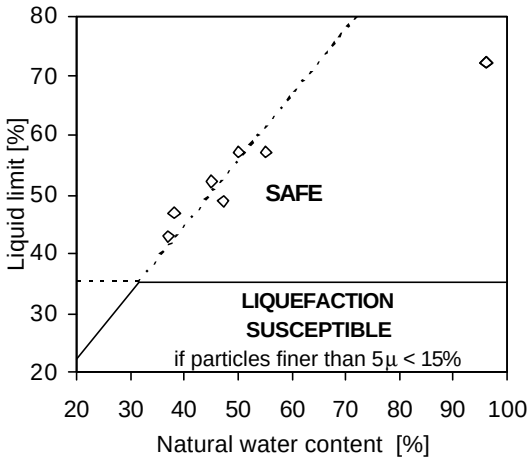

Fig. 15. Evaluation of Chinese criteria

ACKNOWLEDGMENT

The partial financial support of Bogazici University Research Fund under the project no. 03HA402 is greatfully acknowledged.

REFERENCES

[1] O. Yilmaz and M. Eser, "A unified workflow for engineering seismology," in *Expanded Abstracts, 72nd Annual International Meeting of the Soc. of Expl. Geophys.*, October 12-15, 2002, Salt Lake City.

[2] O. Yilmaz, "Seismic data analysis --- processing, inversion, and interpretation of seismic data," Soc. of Expl. Geophys., Tulsa, OK., 2001.

[3] J. Zhang and M. N. Toksoz, "Nonlinear refraction traveltime tomography," Geophysics, **63**, 1726-1737, 1998.

[4] C. B. Park, R. D. Miller, and J. Xia, "Multichannel analysis of surface waves," Geophysics, **64**, 800-808, 1999.

[5] Andresen A.A. and Kolstad P. "The NGI 54-mm samplers for undisturbed sampling of clays and representative sampling of coarser materials" Proc. of the Int. Sym. on Soil Sampling, Singapore, 13-21, 1979.

[6] Li, X. S., Chan C. K., and Shen C. K. "An automated triaxial testing system. Advanced Triaxial Testing of Soil and Rock," ASTM STP 977, ASTM, Philadelphia, 95-106, 1988.

[7] Boulanger, R.W., Meyers, M.W., Mejia, L.H., and Idriss, I.M. "Behaviour of a fine grained soil during the Loma Prieta earthquake" Canadian Geotechnical Journal, vol.35, 146-158, 1998.

[8] Perlea, V.G. "Liquefaction of cohesive soils. Soil Dynamics and Liquefaction 2000", the 2000 specialty conference, Denver, ASCE geotechnical special publication no.107, 58-75, 2000.

[9] Seed, H.B.and Idriss, I.M. "Ground motions and soil liquefaction during earthquakes" EERI Monograph, Berkeley, California,1982.

[10] Youd, T.L. "Screening guide for rapid assessment of liquefaction hazard at highway bridge sites", Multidisciplinary Center for Earthquake Engineering Research Technical Report MCEER-98-0005, 58pp, 1998.

[11] Sancio R.B., Bray J.D., Reimer M.F., and Durgunoglu H.T. "An assessment of the liquefaction susceptibility of Adapazari silt", Proc. of 2003 Pacific Conference on Earthquake Engineering, 2003.

[12] Kalafat M., Emrem C, Durgunoglu H.T. "Behaviour of soft Riva clay under high cyclic stresses", Proc. of Int. Conference on New Developments in Soil Mechanics and Geotechnical Engineering, Lefkosa, 177-183, 2003.